Pis'ma v ZhETF, vol. 102, iss. 11, pp. 811 – 816

Germanium–vacancy color center in isotopically enriched diamonds synthesized at high pressures[1)]

E. A. Ekimov[+], *S. G. Lyapin*[+], *K. N. Boldyrev*[*], *M. V. Kondrin*[+], *R. Khmelnitskiy*[×], *V. A. Gavva*[°], *T. V. Kotereva*[°], *M. N. Popova*[* 2)]

[+] *Institute for High Pressure Physics of the RAS, 142190 Troitsk, Russia*

[*] *Institute of Spectroscopy of the RAS, 142190 Troitsk, Russia*

[×] *Lebedev Physics Institute of the RAS, 117924 Moscow, Russia*

[°] *Institute of Chemistry of High-Purity Substances of the RAS, 603950 Nizhny Novgorod, Russia*

Submitted 15 October 2015
Resubmitted 27 October 2015

We report on the high-pressure synthesis of novel nano- and microcrystalline diamonds with germanium-vacancy (Ge–V) color centers emitting at 602 nm. The synthesis was carried out in non-metallic growth systems C–H–Ge and C–H–O–Ge enriched with germanium and carbon isotopes. We demonstrate germanium and carbon isotope shifts in the fine structure of the luminescence, which allows us to unambiguously associate the center with the germanium impurity entering into the diamond lattice. We show that there are two ground-state energy levels with the separation of 0.7 meV and two excited-state levels separated by 4.6 meV in the electronic structure of the center and suggest a split-vacancy structure of this center. High-intensity and narrow-line emission of high-pressure synthesized small diamonds with Ge–V centers makes them promising candidates for single-photon emitters.

DOI: 10.7868/S0370274X15230022

During the last decade, color centers in diamond have become an object of very intense study in the context of their possible use as luminescent markers in biology [1, 2], for measuring weak magnetic fields with high spatial resolution [1, 3] and, the most important, as three-level Λ systems [4–7] and single-photon emitters [8–11] for quantum information processing and communication (QIPC) technologies. In particular, nitrogen-vacancy (N–V) [8], silicon-vacancy (Si–V) [9], Cr-related [10], and Ni-related (NE8) [11] centers in diamond were shown to be capable of single-photon emitting. The search and study of new photoluminescent centers in diamond is of great importance not only for expanding the spectral range of single-photon emitters, but also for understanding the relationship between the structure and energy level scheme and luminescent properties of color centers in diamond, which is essential for designing an efficient platform for QIPC. In the theoretical paper by Goss [12], it was predicted that germanium, an element with larger than for silicon atomic radius, can form a Ge–V color center in diamond with structure similar to that of the Si–V center and emit photons in the same spectral range. Recently, luminescence at a wavelength of about 602 nm, different from the near-infrared spectral region of the Si–V center, was reported for diamond doped with germanium by ion implantation and in the process of chemical vapor deposition (CVD) [13]. It was demonstrated that the "602 nm" center works as a single-photon source, whereas the nature of the center was not actually established in the presence of other impurities. Luminescence at 602 nm of CVD diamond remained broad even at 5 K indicating imperfect structure of the crystal [13, 14].

High-pressure, high-temperature (HPHT) synthesis is historically known for producing diamond crystals of a very high optical quality. For instance, fine structure in the luminescence line of the Si–V center at 737 nm was first investigated on Si-doped diamond crystals grown by the temperature-gradient method in metallic melts [15, 16]. In practical terms, the size of diamond crystals with single-photon emitters is desirable to be less than the emission wavelength to provide an optimal performance of the emitter [17]. In this regard, HPHT technology was shown to be very efficient for the massive synthesis of pure [18, 19] and doped [20, 21] nanodiamonds from organic compounds. As for germanium impurity,

[1)] See Supplemental material for this paper on JETP Letters suite: www.jetpletters.ac.ru.

[2)] e-mail: popova@isan.troitsk.ru

nothing is known about its presence in diamond grown at high pressures, even from a germanium melt [22]. In this context, HPHT synthesis of Ge-doped diamonds becomes very important not only for elucidating the nature of the "602 nm" luminescent center, but also for producing a platform of appropriate size for new single-photon emitters. It is also worth mentioning that the ^{73}Ge isotope possesses a nonzero nuclear spin ($I = 9/2$) and, thus, a hyperfine structure of energy levels, which could be used to build a three-level Λ system for some QIPC applications.

Here, we describe HPHT synthesis of small high-quality diamond crystals with Ge-related color centers in the C–H–Ge growth system. HPHT diamond synthesis from hydrocarbons became the basis for producing small diamond crystals with a high structural perfection. Naphthalene, $C_{10}H_8$, mixed with germanium was used for the synthesis of germanium-doped diamonds (Fig. 1). Similar to the synthesis of diamond from pure

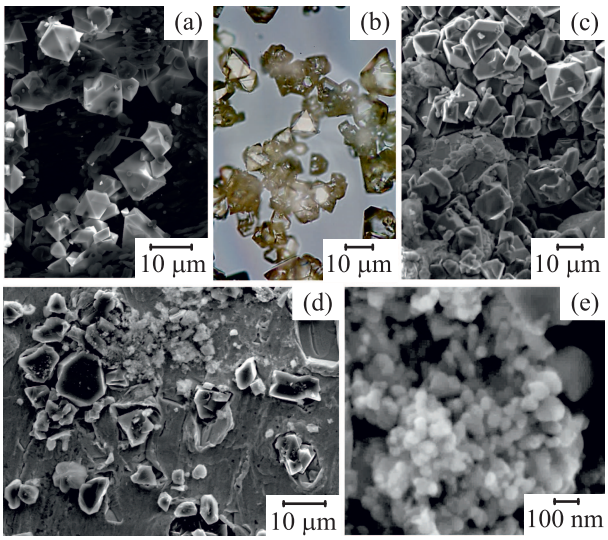

Fig. 1. (Color online) Microcrystals of up to 10–15 μm in size with perfect shape were obtained under the pressure 7–8 GPa (a, b), while at a higher pressure, 8–9 GPa, the formation of diamond nanocrystals of 30 to 100 nm in size was revealed among microcrystalline diamonds (c–e): microdiamonds as-synthesized (a) and after an acid treatment (b). (c) – Micro- and nano-sized diamonds in as-synthesized sample. (d) – Acid-treated micro- and nano-sized diamonds placed on the indium plate. (e) – Nano-sized diamonds (enlarged part taken from the previous image). Panels a, c, d, e are backscattered electron images, while b is an optical microscope one

naphthalene [23], diamond formation in the Ge–C–H growth system at 8–9 GPa takes place at temperatures above 1600 K. At these temperatures germanium does not act as a catalyst for the diamond synthesis [22], which makes it possible to control doping of diamond by changing concentration of germanium in the growth system. Powders of Ge-doped diamond crystals were synthesized using carbon and germanium with natural isotopic composition, 99 % ^{12}C and n-Ge (36.5 % ^{74}Ge, 27.4 % ^{72}Ge, 20.5 % ^{70}Ge, 7.8 % ^{73}Ge, 7.8 % ^{76}Ge), respectively, as well as those enriched with the isotopes ^{13}C (99.3 at. %), ^{72}Ge (99.98 %) or ^{76}Ge (88 % ^{76}Ge, 12 % ^{74}Ge). Ge-doped diamonds with different germanium isotopic composition were produced from powder mixtures of naphthalene ($C_{10}H_8$, 99 % ^{12}C) and germanium (0.7, 4, and 13 mass %). The mixtures were prepared in a mixer (mortar and pestle, both made of jasper or plexiglass) for about 5 min, pressed into pellets, and placed inside titanium capsules. For diamond synthesis, toroid-type high-pressure chamber was used to generate pressures 7–9 GPa and a desired temperature between 1600 and 1900 K in the reaction volume. Under pressure, total duration of the heat treatment was about 10 s. After the treatment, samples were quenched under pressure to room temperature by switching off the electric power. Then, powdered samples were recovered from the capsules and treated consequently in aqua regia, solution of nitric and sulfuric acids (1:3), and perchloric acid to remove nondiamond phases from the samples. All crystals obtained were transparent; neither non-diamond phases nor metallic impurities were detected in acid-treated powder samples by x-ray phase and EDX analysis (see Fig. S1 in [24]). Diamond enriched with isotope ^{13}C was synthesized from ^{13}C amorphous carbon. Since synthesis of diamond in the growth system n-Ge(13 mass %)–^{13}C amorphous carbon caused uncontrollable Ge-doping of diamond and trapping of germanium-based inclusions (see Fig. S1 in [24]), H_2O (12 mass %) was added to the mixture in order to prevent synthesis of diamond in the double Ge–C system. Unlike the case of the base C–H–Ge growth system, crystal structure of diamond synthesized in the presence of water was less perfect.

Photoluminescence (PL) spectra were recorded using the 488 nm Ar^+ laser line for excitation and a triple-grating spectrometer (Princeton Instruments TriVista 555) with a liquid-nitrogen-cooled CCD detector. For measurements in the temperature range 80–300 K, the samples were placed inside a cryostage (Linkam THMS600) and a 50× objective (NA = 0.50) of a confocal microscope (Olympus BX51) was used to focus the laser beam and to collect the PL signal. To perform measurements at 10 K, the samples were put into a He cryostat (Oxford Instruments OptistatSXM) and an achromatic lens was used for focusing the laser beam

and collecting the signal. The laser spot on the sample inside the cryostat was about 5 μm. Low-resolution (~ 0.25 meV $= 0.1$ nm) spectra covering the entire sideband were measured using a spectrometer in subtractive configuration with a 600-grooves-per-mm grating. A zero-phonon line (ZPL) was measured with a 1800-grooves-per-mm grating in additive configuration which gave a ~ 0.03 meV (~ 0.01 nm) resolution capable of resolving the fine structure of four lines, separated by ~ 0.7 and ~ 4.6 meV and with typical full width at half maximum FWHM $= 0.1$–0.4 meV.

Density functional theory (DFT) calculations were carried out with Quantum ESPRESSO software package [25]. Perdew–Burke–Ernzerhof (PBE) exchange correlation functional was applied with norm-conserving pseudopotentials (of the Trouiller–Martins type) for both carbon and germanium atoms. Energy cut-off was 140 Ry. For integration over the Brillouin zone, unshifted $8 \times 8 \times 8$ Monkhorst–Pack grid was used. In the process of calculation, the relaxation of cell dimensions and ion positions was done until the residual force on every atom was less than 0.001 Ry/Bohr and the residual stress was less than 50 MPa. For calculation of the spin-orbital splitting, we used already relaxed supercells with substitution of fully relativistic pseudopotential for germanium only. In this case, only self-consistent calculations were carried out. Due to deficiencies of PBE functionals which regularly underestimate band gaps, the band structure was subsequently corrected by using a hybrid functional (HSE06) with standard parameters (0.25 Å^{-1} for the mixing ratio and 0.2 Å^{-1} for the screening value).

Figs. 2a shows typical photoluminescence spectra collected on diamonds doped with germanium of natural isotope composition (n-Ge). At 300 K, a zero-phonon line was found at 602.5 nm with FWHM 4.5 nm (~ 16 meV). The ZPL, typically 2–10 times stronger in intensity than the diamond Raman line, becomes more intense with increase of the germanium concentration in the growth medium. At 80 K, the ZPL splits into two lines at 602.1 and 601.1 nm with FWHM 0.25 nm (~ 0.9 meV). Further cooling down to 10 K results in a significant narrowing of the lines to 0.1 nm (~ 0.38 meV). ZPL is accompanied by a broad vibronic sideband with a sharp feature at 615 nm (45.2 meV with respect to the ZPL) typical for a localized vibrational mode (LVM), see Fig. 2b. Depending on the synthesis conditions, (Si–V)$^-$ line, (N–V)^0, and (N–V)$^-$ lines could be detected in the spectra, see inset of Fig. 2a and Fig. 2b. The presence of silicon in the growth system was caused by contaminating the initial mixture during its preparation in a jasper mortar. In contrast to the Ge-doped diamond

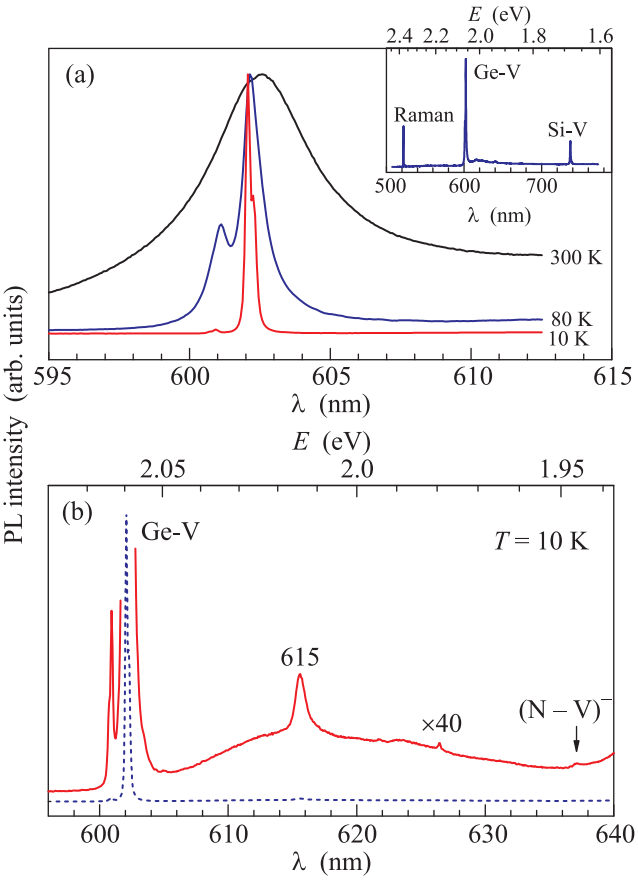

Fig. 2. (Color online) Photoluminescence spectra of Ge-doped diamond. (a) – Splitting of the "602 nm" line with cooling from 300 to 80 and 10 K. Inset shows a PL spectrum at 80 K with all three dominating features: ZPL at 602 nm, the Raman peak from diamond and the Si–V line at 737 nm. (b) – Sideband structure near the ZPL revealing 615 nm localized vibrational mode, besides the (N–V)$^-$ peak at 637 nm. The sideband intensity is multiplied by a factor 40

films [13, 14], the presence of silicon impurity in our Ge-doped diamonds was easily eliminated by using a plexiglass mortar instead of a jasper one (see Fig. S2 in [24]). The presence of (N–V)^0 and (N–V)$^-$ peaks in the luminescence spectra of diamonds was revealed only at cooling down to 80 K. Interestingly that boron, if added to the growth system, lowers nitrogen concentration in diamond to a level undetectable in luminescence spectra, as well as decreases FWHM of the luminescent line at 602 nm. Thus, simple manipulations in chemical composition of starting mixtures make it possible to govern the luminescence spectrum of HPHT diamonds.

High-resolution spectra recorded at 10 K reveal the four-line fine structure of ZPL (Fig. 3a), which can be interpreted in terms of optically allowed transitions between the doublet ground and excited states (Fig. 3c)

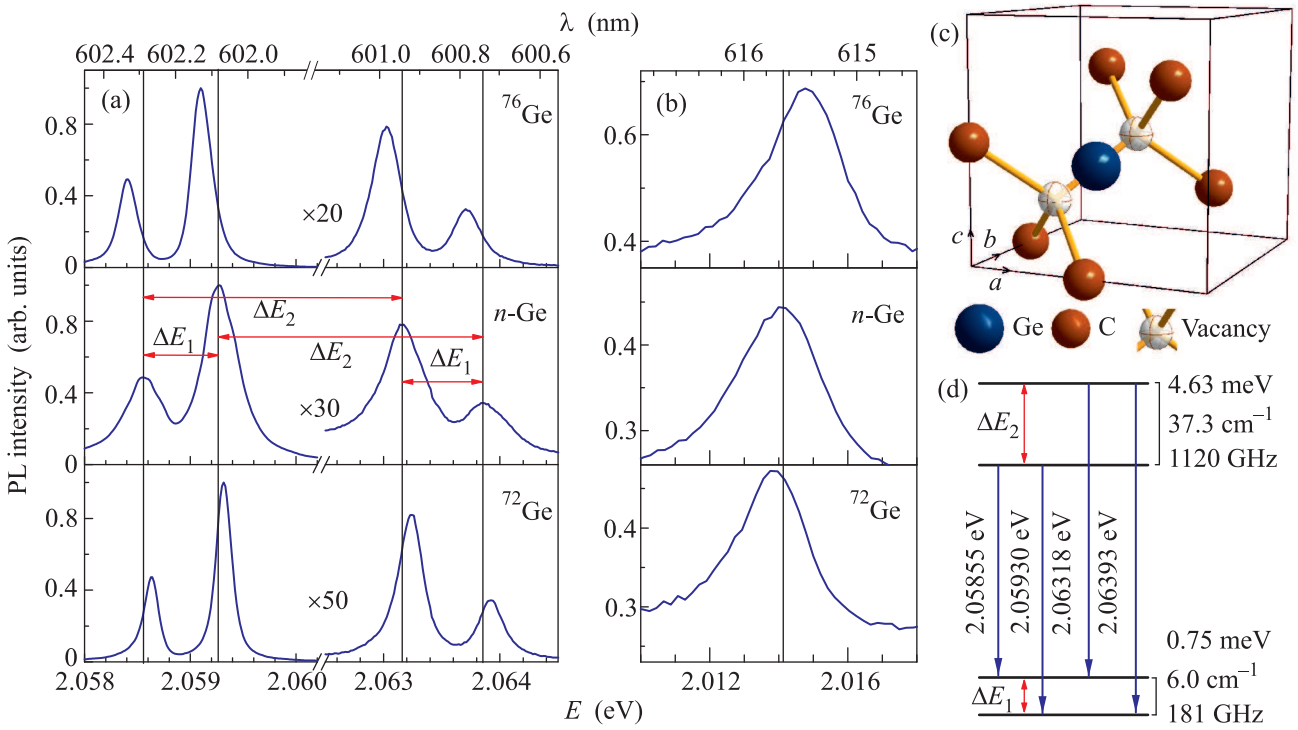

Fig. 3. (Color online) Isotopically varying spectral features of the Ge center in diamond. (a) – High-resolution spectra of the 602 nm Ge-related peak reveal two doublets, which shift to a lower energy as the Ge atom increases in mass. Note that replacing natural Ge by isotopically pure ^{72}Ge results in an extraordinary narrowing of ZPL down to 0.05 nm (∼0.16 meV). (b) – Sharp LVM peak at 615 nm moves to higher energy as the Ge mass increases. The actual energy of the localized vibrational mode is given by the separation between this peak and the zero phonon line, and therefore the LVM energy decreases for *n*-Ge and ^{76}Ge. (c) – The split-vacancy configuration of the Ge–V center with the Ge atom (blue) in between the unoccupied lattice sites (white) and the nearest-neighbour carbon atoms (red). (d) – Energy-level scheme of the Ge–V center. The split ground and excited states give rise to four optical transitions presented at panel a

in the same manner as for the fine structure of ZPL in the case of the Si–V center [16]. In total, more than twenty micro-sized (3–9 μm) and aggregated nano-sized (30–100 nm) diamonds were studied at 80 K. No significant variation in the position of ZPL was detected, while FWHM of the ZPL became smaller at low germanium concentration.

To prove that ZPL at 602 nm and LVM at 615 nm originate from the Ge center we have grown samples: i) replacing natural Ge by the ^{72}Ge or ^{76}Ge isotopes and ii) replacing natural carbon by the ^{13}C isotope. In the case i, we observed that all four peaks of the ZPL shift to longer wavelengths as the Ge atom increases in mass (Fig. 3a), which unambiguously associates the nature of the center with the impurity of germanium in diamond. Meanwhile, the distance between the ZPL and the LVM diminishes, in agreement with the phonon energy decrease for a heavier atom. The measured phonon energies for this feature are $E_{\mathrm{LVM}(72)} = 45.43 \pm 0.01$ meV for ^{72}Ge, $E_{\mathrm{LVM}(n\text{-Ge})} = 45.24 \pm 0.01$ meV for *n*-Ge, and $E_{\mathrm{LVM}(76)} = 44.31 \pm 0.01$ meV for ^{76}Ge. We calculated the ratios of the LVM energies and compared them with the ratio of the isotope masses, following the direction of Ref. [26] for the Si–V centre:

$$\frac{E_{\mathrm{LVM}(n\text{-Ge})}}{E_{\mathrm{LVM}(76)}} = 1.0210 \pm 0.0003 \sim 1.0207 = \sqrt{\frac{m^*_{76}}{m_{n\text{-Ge}}}},$$

$$\frac{E_{\mathrm{LVM}(72)}}{E_{\mathrm{LVM}(76)}} = 1.0254 \pm 0.0003 \sim 1.0255 = \sqrt{\frac{m^*_{76}}{m_{72}}}.$$

Here, m^*_{76} and $m^*_{n\text{-Ge}}$ are the effective masses of the used germanium isotopes (about the effective masses see [24]). The measured ratios are in close agreement with a simple harmonic oscillator model where the phonon frequency ω is given by $\omega = \sqrt{k/m}$. The spring constant k and an oscillating mass m refer to the germanium atom. The validity of this simple approach indicates that the 615 nm spectral feature arises from oscillations of the Ge atom, carbon atoms of the diamond lattice being not much involved.

This conclusion is further supported by our results on the samples ii. On changing the ^{13}C content from

1.1 % in natural carbon to 99 %, we observed the isotope shift +2.8 meV for the ZPL (see Fig. 3S in [24]), while the energy of the LVM does not noticeably change with carbon isotopic substitution. These observations are consistent with a model of a strongly localized state of a heavy Ge atom in the diamond lattice.

Using DFT calculations performed on a hexagonal supercell of 84 atoms with the [0001] direction parallel to the ⟨111⟩ direction of the diamond lattice, we show that the structure of the Ge–V defect is consistent with the split-vacancy model proposed for the Si–V defect [27, 28]. Upon relaxation of atomic positions in the supercell, a germanium atom moves halfway in the direction to the nearby vacant cite. The resulting band structure near the top of the valence band in the Γ point of Brillouin zone is schematically shown in Fig. 4. In this energy range, two doubly-degenerate defect levels are present. Experimentally observed photoluminescence can be explained by transitions between a partially occupied level deep in the band gap and the one close to the top of the valence band. For the $(\text{Ge–V})^{-1}$ centre, the energy-level difference was calculated to be 1.91 eV, whereas the electron excitation energy (calculated using inverse population of energy levels) yields higher energy of 2.01 eV, close to that observed experimentally. The energy splitting values due to the spin-orbit coupling were found to be of about 10 meV for the lower energy pair and about 2 meV for the upper one, while Jahn–Teller splitting values were of the order of 1 meV. Since the energy difference below 10 meV is at the brink of possibilities of DFT, values for energy level splitting must be considered as an order of magnitude estimate only.

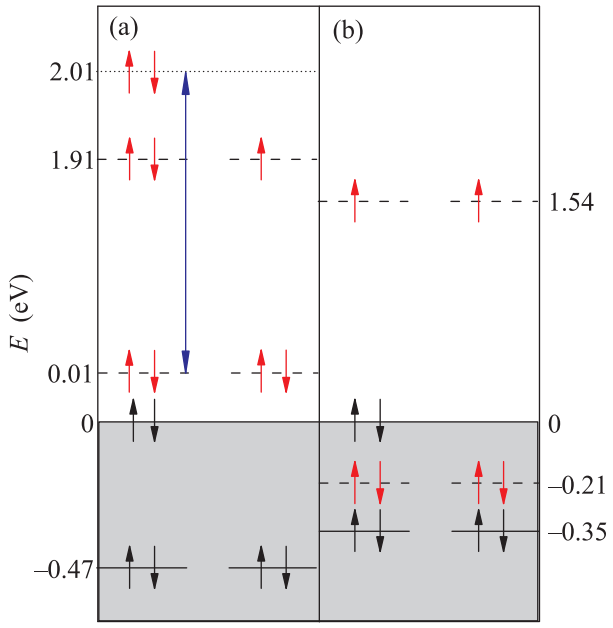

Fig. 4. (Color online) Schematic representation of energy levels of the charged impurity center $(\text{Ge–V})^{-1}$ (a) and the neutral impurity center $(\text{Ge–V})^{0}$ (b) in the vicinity of the valence band maximum. The grey area represents the valence band. Solid lines stand for a triply-degenerate level at the top of the pure diamond valence band (T_{2g}) which is split by the impurity. Dashed lines indicate doubly-degenerate $(\text{Ge–V})^{x}$ impurity levels (for clarity, we neglect the spin-orbital coupling which is at most of the order of 10 meV). Dotted line at the left panel designates an excited state of the Ge impurity. Arrows show occupation of respective levels by electrons. The double-sided arrow at the left panel demonstrates an electronic transition responsible for the observed photoluminescence

In summary, we demonstrate a great potential of the HPHT technology in preparation of small high-quality diamonds with color centers, which can be used as a platform for single-photon emitters and other devices for quantum information processing and communication applications. By detecting carbon and germanium isotope shifts in the luminescence of diamond at 2 eV and its vibrational sideband, we show that germanium enters into the diamond lattice forming Ge-related color center. Similarities in the electronic structure of Ge- and Si-related color centers, as well as our DFT calculations strongly support split-vacancy nature of the Ge-related center in diamond.

We note that after this work has already been performed and prepared for publication a paper [29] appeared reporting on the luminescence of micro-sized diamond crystals synthesized from a germanium-carbon system under high pressure and high temperature. The luminescence spectra demonstrate well resolved structure of ZPL [29], the same as in our study. However, as the authors of Ref. [29] used germanium with natural abundance of isotopes, they could not determine the nature of the Ge-related center unambiguously, in particular, their results did not allow to distinguish between Ge entering the diamond lattice and located on the surface.

The authors acknowledge financial support from the Russian Academy of Sciences under the Programs for Basic Research, Russian Foundation for Basic Research, Projects (15-02-05603 and 13-02-01091) and the President of the Russian Federation (Project # MK-3521-2015.2). The authors thank V.G. Ralchenko for helpful discussions.

1. I. Aharonovich, A. D. Greentree, and S. Prawer, Nat. Photon. **5**, 397 (2011).
2. H. Zhang, I. Aharonovich, D. R. Glenn, R. Schalek, A. P. Magyar, J. W. Lichtman, E. L. Hu, and R. L. Walsworth, Small **10**, 1908 (2014).

3. G. G. Balasubramanian, P. Neumann, D. Twitchen, M. Markham, R. Kolesov, N. Mizuochi, J. Isoya, J. Achard, J. Beck, J. Tissler, V. Jacques, P. R. Hemmer, F. Jelezko, and J. Wrachtrup, Nat. Mat. **8**, 383 (2009).
4. M. V. Gurudev Dutt, L. Childress, L. Jiang, E. Togan, J. Maze, F. Jelezko, A. S. Zibrov, P. R. Hemmer, and M. D. Lukin, Science **316**, 1312 (2007).
5. H. Bernien, B. Hensen, W. Pfaff, G. Koolstra, M. S. Blok, L. Robledo, T. H. Taminiau, M. Markham, D. J. Twitchen, L. Childress, and R. Hanson, Nature **497**, 86 (2013).
6. K. Heshami, Ch. Santori, B. Khanaliloo, C. Healey, V. M. Acosta, P. E. Barclay, and C. Simon, Phys. Rev. A **89**, 040301(R) (2014).
7. E. Poem, C. Weinzetl, J. Klatzow, K. T. Kaczmarek, J. H. D. Munns, T. F. M. Champion, D. J. Saunders, J. Nunn, and I. A. Walmsley, Phys. Rev. B **91**, 205108 (2010).
8. J. Wrachtrup and F. Jelezko, J. Phys.: Cond. Mat. **18**, S807 (2006).
9. E. Neu, D. Steinmetz, J. Riedrich-Möller, S. Gsell, M. Fischer, M. Schreck, and C. Becher, New J. Phys. **13**, 025012 (2011).
10. I. Aharonovich, S. Castelletto, B. C. Johnson, J. C. McCallum, D. A. Simpson, A. D. Greentree, and S. Prawer, Phys. Rev. B **81**, 121201 (2010).
11. T. T. Gaebel, I. Popa, A. Gruber, M. Domhan, F. Jelezko, and J. Wrachtrup, New J. Phys. **6**, 98 (2004).
12. J. P. Goss, P. R. Briddon, M. J. Rayson, S. J. Sque, and R. Jones, Phys. Rev. B **72**, 035214 (2005).
13. T. Iwasaki, F. Ishibashi, Y. Miyamoto, Y. Doi, S. Kobayashi, T. Miyazaki, K. Tahara, K. D. Jahnke, L. J. Rogers, B. Naydenov, F. Jelezko, S. Yamasaki, S. Nagamachi, T. Inubushi, N. Mizuochi, and M. Hatano, Sci. Rep. **5**, 12882 (2015).
14. V. G. Ralchenko, V. S. Sedov, A. A. Khomicha, V. S. Krivobok, S. N. Nikolaev, S. S. Savin, I. I. Vlasov, and V. I. Konov, Bulletin of the Lebedev Physics Institute **42**, 165 (2015).
15. G. Sittas, H. Kanda, I. Kiflawi, and P. M. Spear, Diamond Relat. Mater. **5**, 866 (1996).
16. C. D. Clark, H. Kanda, I. Kiflawi, and G. Sittas, Phys. Rev. B **51**, 16681 (1995).
17. I. Aharonovich, S. Castelletto, D. A. Simpson, C.-H. Su, A. D. Greentree, and S. Prawer, Rep. Prog. Phys. **74**, 076501 (2011).
18. R. H. Wentorf, Jr., J. Phys. Chem. **69**, 3063 (1965).
19. A. Onodera, K. Suito, and Y. Morigami, Proc. Jpn. Acad. B **68**, 167 (1992).
20. E. A. Ekimov, O. S. Kudryavtsev, A. A. Khomich, O. I. Lebedev, T. A. Dolenko, and I. I. Vlasov, Adv. Mater. **27**, 5518 (2015).
21. V. A. Davydov, A. V. Rakhmanina, S. G. Lyapin, I. D. Il'ichev, K. N. Boldyrev, A. A. Shiryaev, and V. N. Agafonov, JETP Lett. **99**, 585 (2014).
22. H. Kanda, M. Akaishi, and S. Yamaoka, Appl. Phys. Lett. **65**, 784 (1994).
23. V. A. Davydov, A. V. Rakhmanina, V. Agafonov, and V. N. Khabashesku, Carbon **90**, 231 (2015).
24. See Supplemental material for this paper on JETP Letters suite: www.jetpletters.ac.ru.
25. P. Giannozzi, S. Baroni, N. Bonini, M. Calandra, R. Car, C. Cavazzoni, D. Ceresoli, G. L. Chiarotti, M. Cococcioni, I. Dabo, A. Dal Corso, S. Fabris, G. Fratesi, S. de Gironcoli, R. Gebauer, U. Gerstmann, C. Gougoussis, A. Kokalj, M. Lazzeri, L. Martin-Samos, N. Marzari, F. Mauri, R. Mazzarello, S. Paolini, A. Pasquarello, L. Paulatto, C. Sbraccia, S. Scandolo, G. Sclauzero, A. P. Seitsonen, A. Smogunov, P. Umari, and R. M. Wentzcovitch, J. Phys.: Cond. Mat. **21**, 395502 (2009).
26. A. Dietrich, K. D. Jahnke, J. M. Binder, T. Teraji, J. Isoya, L. J. Rogers, and F. Jelezko, New J. Phys. **16**, 113019 (2014).
27. J. P. Goss, R. Jones, S. J. Breuer, P. R. Briddon, and S. Öberg, Phys. Rev. Lett. **77**, 3041 (1996).
28. A. Gali and J. R. Maze, Phys. Rev. B **88**, 235205 (2013).
29. Y. N. Palyanov, I. N. Kupriyanov, Y. M. Borzdov, and N. V. Surovtsev, Sci. Rep. **5**, 14789 (2015).